ROYAL SOCIETY
OF CHEMISTRY

Advancing cerumen analysis: exploring innovative vibrational spectroscopy techniques with respect to their potential as new point-of-care diagnostic tools†

Edoardo Farnesi, [ID] ‡[a,b] Matteo Calvarese,‡[b] Chen Liu,[a,b] Carl Messerschmidt,[b] MohammadSadegh Vafaeinezhad, [ID] [a] Tobias Meyer-Zedler, [ID] [b] Dana Cialla-May,[b] Christoph Krafft, [ID] [b] Jonas Ballmaier, [ID] [c] Orlando Guntinas-Lichius, [ID] [c] Michael Schmitt [ID] [a] and Jürgen Popp [ID] *[a,b]

Cerumen, commonly known as earwax, is a complex mixture composed of secretions from ceruminous glands. These secretions are heterogeneous mixtures mainly composed of lipids and proteins. Despite its prevalence, the potential diagnostic value of cerumen remains largely unexplored. Here, we present an in-depth analysis of cerumen utilizing well-known vibrational approaches such as conventional Raman spectroscopy or surface-enhanced Raman spectroscopy (SERS) together with advanced vibrational spectroscopy techniques such as coherent Raman scattering (CRS), *i.e.* broadband coherent anti-Stokes Raman scattering (CARS) or stimulated Raman scattering (SRS), as well as optical photothermal infrared (OPTIR) spectroscopy. Through the integration of these vibrational spectroscopic methods, lipids and proteins can be identified as the main components of cerumen; however, they contribute to the final spectral information to various extents depending on the vibrational detection scheme applied. The inherently weak Raman signal could be enhanced by linear (SERS) and non-linear (CRS) processes, resulting in efficient acquisition of fingerprint information and allowing for the detection of marker modes, which cannot be addressed by conventional Raman spectroscopy. OPTIR spectroscopy provides complementary information to Raman spectroscopy, however, without the contribution of a fluorescence background. Our findings underscore the utility of these cutting-edge techniques in unveiling the intricate molecular landscape of cerumen, paving the way for novel point-of-care diagnostic methodologies and therapeutic interventions.

*[a]Institute of Physical Chemistry (IPC) and Abbe Center of Photonics (ACP), Friedrich Schiller University Jena, Member of the Leibniz Centre for Photonics in Infection Research (LPI), Helmholtzweg 4, 07743 Jena, Germany.
E-mail: juergen.popp@uni-jena.de*
[b]Leibniz Institute of Photonic Technology, Member of Leibniz Health Technologies, Member of the Leibniz Centre for Photonics in Infection Research (LPI), Albert-Einstein-Straße 9, 07745 Jena, Germany
[c]Department of Otorhinolaryngology-Head and Neck Surgery, Jena University Hospital, 07747 Jena, Germany
†Electronic supplementary information (ESI) available. See DOI: https://doi.org/10.1039/d4an00868e
‡These authors contributed equally.

Introduction

In point-of-care personalized medicine, accurately detecting diseases in early stages is one of the crucial challenges. Prompt diagnosis leads to successful and rapid therapy, which surely improves the prognosis of a patient, increases the probability of survival and also results in better quality of life.

The quest for progress in point-of-care diagnostics has recently gained momentum in the field of liquid biopsy, which seeks to provide a valid and reliable assay for diagnosing and identifying illnesses from body fluids.[1,2] Since any change in homeostatic balance alters the status of human health, the analysis of biological fluids provides a fast, reliable and non-invasive way to reflect what is occurring inside an affected body. Moreover, these point-of-care trials are of pivotal importance, as some disease-associated biomarkers can be found in peripheral biomatrices at the very early stage of pathology when successful therapies and the improvement of patient survivability are much more likely.[3] Numerous studies have been conducted over the past decades on countless diseases, especially cancer, exploring clinically relevant body fluids for the detection and follow-up of pathologies such as oral cancer,[4] pancreatic cancer,[5] lung cancer,[6] ovarian cancer,[7] and

breast cancer.[8] Point-of-care biomarker tests for non-blood fluids (*e.g.* saliva, urine, stool, tears, sweat, breath, seminal fluid, and cerumen) are not yet available for all of these matrices and require further research before translation into routine clinical procedures.[9]

Cerumen, a yellowish waxy substance that is often overlooked, plays a crucial role in the health and functionality of the auditory canal. Composed of a heterogeneous mixture of lipids (including saturated and unsaturated fatty acids, 60–70%), proteins (high percentage of keratin, 20–30%), and other organic compounds, cerumen serves as a protective barrier, shielding the delicate structures of the ear canal from foreign particles, pathogens, and water.[10–15] Apart from the forensic contexts, *e.g.* post-mortem drug overdose and alcohol abuse evaluations, this body fluid has not been sufficiently valued in clinical diagnostics over time, except in only a few cases. In the diagnosis of some metabolic diseases, such as allergic rhinitis and otosclerosis, some genetic disorders, such as maple syrup urine disease and alkaptonuria, and only recently in detecting breast cancer and some cancer biomarkers, testing has been conducted using earwax.[16,17]

Despite being a neglected body fluid, cerumen is less prone to contamination from ambient air and/or cosmetics, and most importantly, accessing it is easy and the sampling is painless and non-invasive, with a storage time longer than that for other bio-matrices such as saliva, urine and serum.[18]

Traditional methods of cerumen analysis have primarily focused on physical characteristics such as color, texture, and odor, offering limited insights into its biochemical composition and potential diagnostic significance.

In recent years, vibrational spectroscopy has emerged as a powerful tool for the non-invasive, label-free analysis of biological samples, enabling detailed molecular characterization with high sensitivity and specificity. Here, we explore to the best of our knowledge for the first time the potential of a multitude of different vibrational spectroscopy techniques in analyzing and characterizing cerumen based on its unique vibrational spectroscopic signature. In detail, we apply Raman spectroscopy (RS), surface-enhanced Raman spectroscopy (SERS), broadband coherent anti-Stokes Raman spectroscopy (BCARS), stimulated Raman scattering (SRS) and optical photothermal infrared (OPTIR) spectroscopy to characterize human cerumen samples. These vibrational spectroscopy techniques are invaluable for a wide range of bioanalytical applications, including disease diagnosis and fundamental biological research.[19–21] RS provides molecular vibrational information, allowing for the identification and characterization of various biomolecules.[22,23] However, the inherently weak Raman signal can sometimes be overwhelmed by background noise, limiting its sensitivity. SERS, on the other hand, overcomes the weak signal intensity of traditional Raman spectroscopy. By leveraging the electromagnetic enhancement by plasmonic nanoparticles, SERS greatly enhances the Raman signal from analytes adsorbed onto the nanoparticle surface. Additionally, a chemical enhancement mechanism is observed in SERS, providing a minor contribution to the overall enhancement of

SERS. The SERS technique has been extensively used to detect trace amounts of biological molecules, enabling sensitive and selective analysis with potential applications in diagnostics and therapeutics.[24,25] BCARS and SRS are nonlinear Raman methods that provide alternative approaches to enhance the Raman signal from weak scatterers, making them suitable for the study of biological samples. Both BCARS and SRS have been proved to be valuable tools for studying lipid metabolism, drug delivery, and other cellular processes, where lipid droplets, lipoproteins, and other lipid-rich structures can be visualized.[26–29] OPTIR spectroscopy is a technique that measures the absorption, reflection, and transmission of infrared light to identify specific functional groups (such as hydroxyl, carbonyl, and amide groups present in lipids, proteins, and carbohydrates) in biomolecules, providing detailed information about molecular structures, hydrogen bonding, and conformational changes.[30,31]

Comparing the outputs from RS, SERS, BCARS, SRS and OPTIR spectroscopy, and leveraging the unique strengths of each spectroscopic technique, we aim to unravel the complex molecular architecture of cerumen, shedding light on its biological functions and diagnostic implications. This first comprehensive vibrational spectroscopic study of cerumen aims to advance the frontier for the development of new clinical diagnosis methods using non-invasive techniques and an easily collected biomatrix.

Materials and methods

Cerumen sample preparation

Cerumen samples (Fig. 1) were collected from two healthy individuals. This study was approved by the Jena University Hospital Ethics Committee (RAMTUMAR study; no. 2021-2305-Material), and all volunteers provided written informed consent for enrolling in this study. By limiting our investigation to two specimens, we were able to focus on carefully characterizing the collected spectra, ensuring that any observed patterns or anomalies could be confidently attributed to the inherent properties of the cerumen rather than to inter-sample variability.
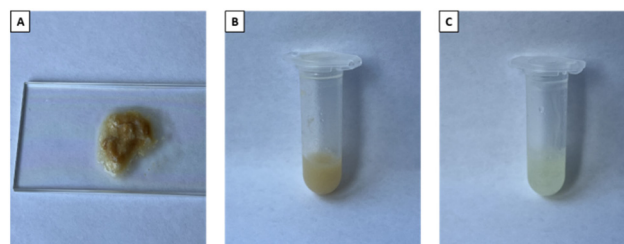

Fig. 1 Cerumen specimens analyzed using vibrational techniques. (A) Human semi-solid cerumen on a microscope glass slide. (B) Human liquid cerumen after pre-processing preparation, *i.e.* supernatant. (C) Artificial cerumen.

Around 50–100 mg of earwax from both ears of each individual were collected in the hospital without damaging the ear canal and immediately stored at −80° C until vibrational spectroscopic analysis. Through visible inspection, only samples with no sign of blood contamination were used for measurement. After thawing at room temperature, cerumen samples were analyzed both directly in their typical sticky semi-solid condition and under liquid conditions after solubilization. For this pre-processing part, samples were transferred to 1.5 mL centrifuge tubes and 0.5 mL of PBS was added to the tube, following an established procedure taken from the literature.[32,33] After 1 h of sonication at 36 °C, the samples were centrifuged at 13 000g for 10 min, and then each supernatant was transferred to a new tube, ready for measurements.

Human earwax has been compared with artificial cerumen (Pickering Laboratories, Mountain View, CA, USA) representing the lipid component of naturally secreted cerumen. It contains oleic acid (20% w/w), linoleic acid (20% w/w), lanolin (20% w/w), paraffin oil (10% w/w), palmitic acid (20% w/w), and myristic acid (20% w/w).

For RS measurements, semi-solid, artificial and liquid cerumen samples were placed on a silicon chip, while for CARS, SRS and OPTIR analyses, a microscope glass slide was used as the substrate (as illustrated in Fig. 1A).

For SERS analysis, both silver (Ag)-coated and gold (Au)-coated silicon nanopillar substrates (SERStrates™), purchased from Silmeco ApS (Copenhagen, Denmark), were incubated in liquid cerumen within the tubes for 20 min. After incubation, each SERS chip was placed on a microscope glass slide and left to dry slowly at room temperature, thus favoring the leaning process of the vertically oriented and highly packed (~20 pillars per μm^2) nanopillars thanks to the surface tension.

Raman and SERS

RS and SERS measurements were performed using a WITec alpha300 R confocal Raman microscope (Ulm, Germany) equipped with a 785 nm laser as the excitation source. The Raman scattered light was collected using a 10× objective lens. RS spectra were collected in the range of 600 to 3100 cm^{-1}, using a laser power of 50 mW incident on the sample, a 300 grooves per mm grating and an integration time of 5 s with one accumulation. The acquisition was performed over a 2 × 2 mm^2 area in the middle of the deposited sample with a 50-point map (5 points per line and 10 lines per scan).

Setting the laser power on the sample to 5 mW, SERS spectra were recorded using the same Raman instrumentation as described before, within the range of 600 to 2200 cm^{-1}, using a 600 groove per mm grating, a 10× objective lens, and an integration time of 5 s with one accumulation. The acquisition was performed over a 1.5 × 1.5 mm^2 area in the center of the chip with a 150-point map (15 points per line and 10 lines per scan).

Spectral analysis was performed using Origin Pro 2022 (OriginLab, Northampton, MA, USA) software. After removing possible outliers, which show spectral features such as sharp spikes or strong fluorescence background signals, Raman and SERS raw spectra were processed with baseline correction (fifth-order polynomial fit), smoothing, and normalization by area (see Fig. S1 and S2† for the background-corrected Raman and SERS spectra). Mean intensity profiles were obtained for each sample. Band assignment was conducted based on data from the literature.[34–37]

BCARS and SRS

A home-built BCARS platform was used to acquire broadband CARS spectra. The setup, shown in Fig. S3,† employs a multiplex CARS approach in which a narrowband pump pulse at 1032 nm and a broadband Stokes pulse ranging from about 1100 nm to nearly 1600 nm are superimposed on the sample to generate a broadband anti-Stokes signal, containing Raman-spectral information between 700 and 3200 cm^{-1}. A complete description of the setup is included in the ESI†, and Fig. 4A illustrates a simplified diagram of the setup. Broadband CARS spectra of the liquid, semi-solid and artificial cerumen samples were acquired using an average power of 15 mW for the pump pulse and 2 mW for the Stokes pulse at the sample plane, at a repetition rate of 1 MHz. A 20×/NA 0.4 objective lens was applied.

To prevent photodamage to the specimens, the laser focus was scanned across the sample and an image was acquired, with a pixel acquisition time of 20 ms over a 50 × 50 μm^2 field of view. To remove the inherently present non-resonant background (NRB),[38] a Kramers–Kronig (KK) phase retrieval algorithm was employed.[39,40] Before processing, the BCARS images were processed by K-means clustering and the clusters of spectra with highest intensity were averaged. The KK algorithm was then applied to the average spectrum of each sample using a mean BCARS spectrum of the glass slide as the reference NRB.

Stimulated Raman scattering (SRS) spectra of the three samples (see Fig. 1) were acquired using a commercial multi-modal microscopy platform (Stellaris 8, Leica Microsystems GmbH). The microscope is equipped with an SRS detection system and enables the acquisition of broadband SRS spectra in a hyperspectral configuration, *i.e.* the Stokes wavelength is fixed and the pump wavelength is sequentially scanned. The system features a CARS and SRS excitation laser (picoEmerald, A.P.E. GmbH) that provides a Stokes pulse at about 1031 nm and a tunable pump pulse in the 700–990 nm range at a repetition frequency of 80 MHz. For SRS acquisition, the Stokes pulse is modulated at 20 MHz and a lock-in detection system is employed. Fig. 4B illustrates the schematics of the setup.

The three samples (see Fig. 1) were measured by acquiring images over a field of view of 1.55 × 1.55 mm^2, with 512 × 512 pixels, a 3.16 μs pixel acquisition time and using a 10×/NA 0.40 objective (HC PL APO CS2 DRY) for excitation. In the 900–1800 cm^{-1} wavenumber range, the power was set to about 12 mW for the pump pulse and 29 mW for the Stokes pulse. In the CH stretching wavenumber region, due to high signal intensity, the power was reduced to around 4 mW and 8.5 mW for the pump and Stokes pulses, respectively.

K-means clustering was performed on the SRS images to group and average only the spectra with the highest intensity. Being a background-free technique, no further processing, except for a fifth-order polynomial fit baseline correction, was required to retrieve Raman spectral information from the SRS signal.

Fig. S4 and S5† show the raw SRS spectra after K-means clustering and the BCARS spectra after clustering and NRB removal. The SRS spectra clearly show greater variability in the data, which can be attributed to several factors. These include high heterogeneity of the sample surface in the wide FOV, low signal due to sample thickness and short pixel dwell time, and low spatial sampling (more information is provided in the ESI†).

OPTIR spectroscopy

OPTIR spectra and images of cerumen presented in this work were acquired using the mIRage+R™ infrared microscope (Photothermal Spectroscopy Corp., Santa Barbara, CA, USA), controlled by PTIR Studio software. The instrument is equipped with a four-chip pulsed and broadly tunable high-power quantum cascade laser (QCL) covering the spectral ranges of 934–1800 cm^{-1} and 2700 to 2999 cm^{-1} (MIRcat 2400, Daylight) and a 785 nm probe laser (Cobolt). Spectral and imaging data were collected in reflection mode by focusing the IR laser on the sample using a 40×/NA 0.78 reflective Cassegrain-style objective. The power of the QCL IR laser was set to 21% at a 10% duty cycle and the power of the probe laser was set to 37%. Cerumen samples were deposited on microscope glass slides. OPTIR spectra at a resolution of 6.6 cm^{-1} were acquired in high-speed mode at a rate of 1000 cm^{-1} s^{-1} with two averages. All spectra were automatically normalized to the collected background spectrum, as displayed in Fig. S6.† Discrete wavenumber OPTIR images were recorded from 70 × 70 μm^2 regions of interest at a speed of 70 μm s^{-1} and step size 1 μm at 2850 and 1650 cm^{-1}. DC images record the intensity of the probe laser reflection, which resembles white-light images.

Comparison of the measurement techniques

Table 1 compares the different vibrational spectroscopy techniques used in this study to highlight the strengths and weaknesses of each, especially from the perspective of point-of-care

analysis of earwax or body fluids in general. The "Acquisition speed" column refers to that used for measurements in this study. The "Setup/level of maturity" column indicates whether the spectra were acquired using a commercial or homemade setup and to what level of maturity the technique has been developed. The "Background" column indicates whether the techniques inherently show a background signal that must be removed by post-processing to recover spectral information. The "Quantitative analysis" column deals with the possibility of performing quantitative analysis on the chemical composition of samples under examination. It mainly relates to the linearity of the techniques with respect to the concentration of chemical species and their reliability and reproducibility. Since the SRS hyperspectral cube is generated by sequential sweeping of each wavenumber, it is not possible to directly calculate the acquisition time of a spectrum. The table shows the sweeping time required to tune the wavelength, as provided on the official excitation laser documentation page (**https://www.ape-berlin.de/en/cars-srs/#specification**). Laser wavelength tuning time is the limiting factor in hyperspectral SRS, as the actual exposure time can be on the order of ms as for BCARS. Laser systems designed specifically for SRS can achieve a much smaller sweeping time than our system, as low as 5 ms.[41] The QCL is also tuned at a speed to 1000 cm^{-1} per second to collect IR spectra, which gives the minimum collection time of *ca.* 2 s.

Results and discussion

Raman spectroscopy as a vibrational spectroscopic gold standard for the identification of potential diagnostic biomarkers in cerumen

RS serves as a powerful tool for biomolecular analysis. In this section, we report, to the best of our knowledge for the first time, the vibrational characteristics of human semi-solid, human liquid and artificial cerumen using RS. Fig. 2 shows spontaneous Raman spectra of all earwax specimens depicted in Fig. 1 deposited on silicon wafers. All spectra highlight, to a large degree, lipid contributions in both the fingerprint and high-wavenumber regions with the most prominent bands being at 2940, 2888, 2856, 1450, 1298, 1125 and 1060 cm^{-1}. Table 2 provides detailed band assignments as well as the corresponding references.

Table 1 Comparison of the capabilities and characteristics of the different spectroscopic techniques

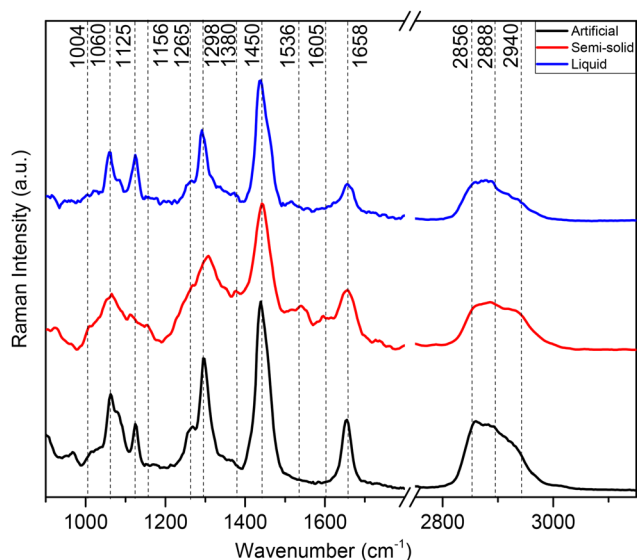| Technique	Acquisition speed	Setup/level of maturity	Background	Quantitative analysis
Raman	5 s per spectrum	Commercial system/high	Fluorescence	Possible and well established
SERS	5 s per spectrum	Commercial system and commercial substrates/high	Fluorescence	Limited reproducibility
Hyperspectral SRS	5 s per spectral point	Commercial system/medium	None	Possible[42]
Multiplex Broadband CARS	20 ms per spectrum	Custom-made system/low	Non-resonant background	Limited due to nonlinear dependence on concentration
OPTIR	2 s per spectrum	Commercial system/medium	None	Possible[30]

Fig. 2 Averaged Raman spectra of earwax samples displayed in Fig. 1. Artificial cerumen (black spectrum), human semi-solid cerumen (red spectrum) and human liquid cerumen (blue spectrum). Wavenumber range between 900 and 3100 cm^{-1}. The spectra are cut in the silent region between 1800 and 2750 cm^{-1}. Spectra are offset for clarity.

At high wavenumbers, the CH$_2$ symmetric stretching vibration of lipids results in the most intense peak at 2856 cm^{-1}, followed by Fermi resonance of the CH$_2$ deformation overtone at 2888 cm^{-1} and anti-symmetric CH$_2$ stretching at 2940 cm^{-1} of lipids, with smaller contributions of proteins. In the fingerprint region, the main Raman peaks are assigned to CH$_2$ scissoring (1450 cm^{-1}) and CH$_2$ in-phase twisting (1298 cm^{-1}) attributed to lipids. Symmetric and asymmetric C–C modes of fatty acid chains show bands at 1060 and

1125 cm^{-1}, respectively. Unsaturated fatty acid chains are evident from C=CH (1265 cm^{-1}) and C=C (1658 cm^{-1}) vibrations. Weaker molecular vibrations typical of proteins are observed only in the semi-solid cerumen spectrum, in particular a shoulder near 1004 cm^{-1} (phenylalanine) and 1658 cm^{-1} (amide I), which slightly broadens the C=C band of lipids. Furthermore, β-carotenoid (1156 and 1536 cm^{-1}) modes are detected in semi-solid cerumen (see Fig. 2, red spectrum). The lipid unsaturation degree can be calculated as the ratio of Raman band intensities at 1660 and 1450 cm^{-1}.[43] Altered secretions of lipids have considerable diagnostic relevance, especially in cancer diagnostics. Increased lipid metabolism results in the most substantial metabolic defect in tumors. Abnormal lipid synthesis contributes to fast cancer cell growth and tumorigenesis. In fact, an increasing number of studies highlight that cancers depend on fatty acid and lipid supply.[44,45] These molecular Raman spectroscopic signatures of cerumen might be used in the future as potential pre- or post-operative diagnostic and prognostic tools in cancer liquid biopsies. The detection of pathological alterations in lipids and proteins through RS relies on changes in the intensity ratio of specific aforementioned Raman peaks associated with these biomolecules. Changes within this unique Raman spectroscopic fingerprint might therefore allow for the identification of molecular signatures indicative of various diseases and pathological conditions within cerumen. Pathophysiological variations in lipids are often accompanied by changes in their relative abundance, composition, and structural properties. These alterations are manifested in Raman spectra as shifts in the intensity ratios of characteristic Raman peaks corresponding to lipid and protein vibrational modes (see Table 2), reflecting underlying biochemical changes associated with disease progression. These changes in Raman intensity ratios may be attributed to vari-

Table 2 Tentative band assignment for the spectra acquired using the different techniques

RS	Ag SERS	Au SERS	BCARS	SRS	OPTIR	Band assignments
			3010			ν(=CH) unsaturated lipids[34,35]
2940			2940	2930	2958	ν_{as}(CH$_3$) proteins/lipids[34,35]
					2920	ν_{as}(CH$_2$) lipids[34,35]
2888			2888	2903		Fermi resonance δ(CH$_2$) lipids[34,35]
2856			2850	2856	2850	ν_{s}(CH$_2$) lipids[34,35]
					1740	ν(C=O) esters lipids[34,35]
1658	1623	1635	1660	1660	1650	ν(C=C) lipids/amide I proteins[36]
	1586	1590				Proteins[34,35]
1536					1545	Raman: carotenoids/IR: amide II
1445	1440	1450	1450	1440	1455	δ(CH$_{2/3}$) lipids/proteins[36]
1380				1380	1382	β(COH) sphingoglycolipids[34]
	1325	1350				Protein AAs[36,37]
1298	1325	1295	1298	1298	1272	τ(CH$_2$) lipids/amide III proteins[34,35]
	1208			1200		Proteins[36]
1156						Carotenoids[34]
1125	1130	1140	1130	1125		ν(C–C) lipids[34,35]
1060			1065		1065	ν(CC) or β(COH) sphingoglycolipids[34,35]
	1004	1000				Protein AAs[36,37]
	824	828				Protein AAs[36,37]
	723					Protein AAs[36]
	660	650				Protein AAs[36]

Key: as – asymmetric, s – symmetric, ν – stretching, δ – deformation, β – in-plane bending, τ – in-phase twisting. AAs – amino acids.

ations in lipid synthesis or the presence of disease-specific biomarkers within earwax samples.

For instance, previous studies showed that RS serves as a valuable tool for detecting lipids and providing insight into their composition and distribution in various pathological conditions, including brain tumors, breast cancer and atherosclerotic plaques. These diseases are commonly characterized by the accumulation of lipids, particularly cholesterol and triglycerides.[46–48] While it presents several advantages, such as non-destructive analysis, chemical specificity, and minimal sample preparation, RS also faces limitations related to signal intensity and possible fluorescence interference. Weak signals, especially for diluted analytes or low-concentration biomarkers in complex biological fluids, limit the detection sensitivity and acquisition speed. Indeed, the Raman spectral analysis of liquid cerumen (blue spectrum, Fig. 2) droplets reveals very weak Raman signals for proteins in the fingerprint wavenumber region. To overcome this limitation, the use of advanced Raman signal enhancement techniques or coherent amplification strategies shows great potential to improve the detection sensitivity of biomarkers for a possible point-of-care diagnosis. Recent advancements in SERS and CRS have advanced the field beyond the capabilities of traditional RS.

Boosting the Raman spectroscopic efficiency with plasmonic and coherent enhancement techniques

SERS analysis. SERS can achieve Raman signal enhancements of several orders of magnitude, effectively overcoming the intrinsic limitations of conventional Raman spectroscopy mentioned above. This increased sensitivity enables the detection of trace-level analytes in complex matrices, surpassing the detection limits of spontaneous Raman spectroscopy by a significant margin.

Here, we performed a SERS analysis of earwax for liquid and artificial cerumen absorbed on Ag-coated and Au-coated silicon nanopillars as SERS substrates. These SERS substrates (purchased from Silmeco ApS, Copenhagen, Denmark) have been chosen due to their high sensitivity. More details about these potent SERS substrates can be found in the literature.[49,50]

As shown in the SEM images (Fig. 3A and B), the leaning mechanism after the air-drying process induces silicon nanopillars to pull together, trapping the cerumen molecules in hot spots. Having the analytes localized in several hot spots is pivotal for a significant enhancement of the earwax Raman signal due to the coupling effect of localized surface plasmon resonances between close nanopillars.[49]

To observe uniform SERS signals, spectra were collected in the central area of the leaning nanopillar chips. Fig. 3C and D shows spectra with the deformation and skeletal CC stretching of amino acids. The SERS signal at 1004 cm^{-1} is characteristic of the ring breathing mode of phenylalanine, and the band at 1130 cm^{-1} corresponds to the CC stretching of fatty acids in lipids.[51] The SERS peaks at 1325 and 1586 cm^{-1} are due to the CH$_2$ in-phase twisting and C=C out-of-phase stretching of
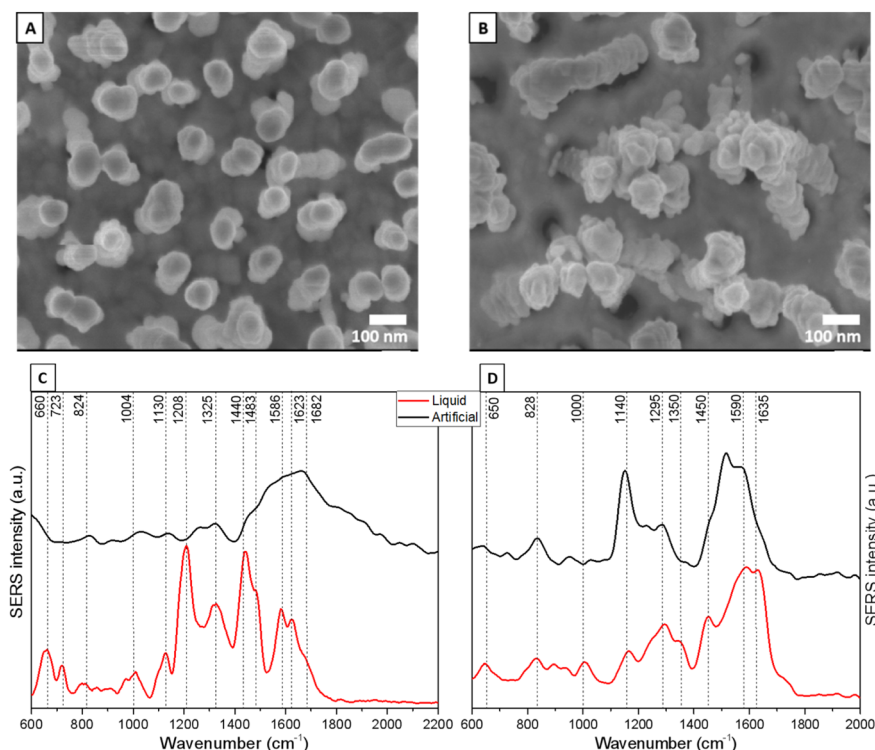

Fig. 3 SEM images of Ag-coated silicon nanopillar substrates (A) before and (B) after their leaning mode due to the drying process. Averaged SERS spectra of artificial (black) and liquid (red) cerumen absorbed, respectively, on (C) Ag-coated and (D) Au-coated SERS substrates. Spectral range: 600–2000 cm^{-1}. Spectra are offset for clarity.

amino acids/lipids, respectively. Moreover, protein amide I (1623 cm^{-1}) and C=C in-phase stretching (1682 cm^{-1}) vibrations of lipids are also visible. In comparison with the artificial cerumen (Fig. 3C, black line), no distinct vibrational pattern was observed for the liquid cerumen from healthy volunteers. One explanation could be the variation in the chemical composition between these two sample classes; moreover, due to the viscous properties of artificial cerumen, the leaning effect of the Ag nanopillars is less pronounced and, thus, the mean SERS spectra show lower intensity, resulting in biochemical feature assignment only in the 1500–1700 cm^{-1} region.

On the other hand, the SERS spectrum of artificial cerumen absorbed on Au nanopillars (Fig. 3D, black line) helps identify fatty acids (*i.e.* palmitic acid) through the characteristic peaks at 1140 cm^{-1} (C–C stretching), 1295 cm^{-1} (CH$_2$ in-phase twisting) and 1590 cm^{-1} (C=C out-of-phase stretching). Other prominent SERS peaks in liquid cerumen (Fig. 3D, red line) are assigned to protein amide I (1635 cm^{-1}), protein/lipid CH deformation or CH$_2$/CH$_3$ bending (1450 cm^{-1}) and protein CH wagging (1350 cm^{-1}). The SERS peaks at 650, 828 and 1000 cm^{-1} are assigned to amino acid COO$^-$ deformation, amino acid C–C stretching and aromatic amino acid ring breathing vibrations, respectively.

Overall, this band assignment shows that cerumen SERS analysis highlights the possible detection of vibrational contributions from two well-known biomarkers traditionally used as point-of-care diagnostic and prognostic tools, namely fatty acids and keratins *via* the SERS bands at 1586 and 1140 cm^{-1} for the fatty acid and 1623, 1350 and 660 cm^{-1} for the protein, respectively. Palmitic acid and keratin, which play a key role in anti-inflammatory processes and in the regulation of lipid metabolism, are cancer biomarkers in neuroblastoma, breast cancer and oral cancer.[52,53] Keratins, with their altered levels in blood, are also extensively recognized as diagnostic tumor markers (*i.e.* epithelial and oral cancers), but increasing evidence has indicated their role as prognostic markers and as active regulators of tumorigenesis.[54]

This difference between the cerumen SERS spectra collected using Ag-coated and Au-coated substrates indicates that specific biochemical components of cerumen that have stronger affinity to either Au or Ag nanopillars dominate the respective spectra, leading to the stark differences observed. These interactions between analytes and metal surfaces can cause shifts in peak positions, changes in intensity as well as their ratio, and even the appearance or disappearance of certain vibrational modes, contributing further to the disparity between the SERS spectra obtained from the two metals.

BCARS and SRS analysis. Coherent Raman scattering (CRS) in a single-wavenumber configuration has emerged in recent decades as a powerful tool for rapid, label-free imaging of biological media by exploiting the vibrational information of a single characteristic Raman peak of large intensity. Its broadband configurations, namely broadband CARS (BCARS) and broadband SRS, combine the high acquisition speed of CRS with the high spectral information content provided by Raman

scattering. In this section, we show the BCARS and broadband SRS spectral characterization of liquid and semi-solid human cerumen and artificial cerumen. The difference between these two techniques mainly lies in how the Raman spectroscopic information is detected. In the BCARS process, the anti-Stokes-scattered signal is collected and spectrally unmixed using a conventional spectrograph. In hyperspectral SRS, specifically in the setup we utilized, the small change in the pump intensity (stimulated Raman loss) is observed by a complex lock-in detection system. A multiplex BCARS approach, like the one we implemented, allows for fast acquisition with exposure times on the order of ms, even for biologically relevant samples.[55] SRS acquisition speed, on the other hand, strongly relies on the wavelength tunability speed of the excitation laser. Faster multiplex SRS approaches with multi-channel lock-in platforms have been already developed but are still limited to few spectral channels.[56]

Despite the slower speed and greater complexity of the detection system, SRS provides a background-free signal that needs no further processing, whereas BCARS requires advanced computational techniques to eliminate the non-resonant four-wave-mixing background. Furthermore, while the BCARS signal shows a quadratic dependency on the density of scatterers in the sample, the detected SRS intensity varies linearly with concentration, thus allowing for greater sensitivity at lower concentrations and possible quantitative analysis similar to that achievable with spontaneous Raman spectroscopy.[42]

The spectral analysis of cerumen recorded using the BCARS and SRS setups depicted in Fig. 4A and B shows the potential of these vibrational techniques to detect lipids, especially in the high-wavenumber region. Consistent with the Raman spectra shown in Fig. 2, spectral contributions of proteins are weak. Here, BCARS spectra (Fig. 4C) highlight the possibility of tracing unsaturated fatty acids present in human cerumen through the characteristic bands of C=C stretching vibration at 1660 cm^{-1} and the =CH stretching vibration at 3010 cm^{-1}, enabling detection of saturated and unsaturated lipids. Moreover, the relative intensity ratio of CARS signals belonging to lipid CH$_2$ and protein CH$_3$ stretching modes (2888 and 2940 cm^{-1}) suggests a clear traceability of protein-to-lipid variations in the human-derived liquid media.[57]

The same spectral trend of the characteristic vibrational bands is detectable in SRS measurements (Fig. 4D), where the peak at 2933 cm^{-1} shows the highest intensity. SRS also allows evaluating the lipid content at around 2850 cm^{-1}, a typical band of the CH$_2$ symmetrical stretching vibration highly abundant in lipids. In the fingerprint wavenumber region, which is dominated by lipid peaks at 1440 and 1663 cm^{-1}, the human earwax SRS spectra also show some peaks assigned to the COH in-plane bending vibration at 1380 cm^{-1}, indicative of sphinglycolipids.[34] Both SRS and BCARS mainly probe fatty acid contributions. The analysis of the BCARS and SRS fingerprint regions shows comparable spectral profiles to those of the Raman spectra plotted in Fig. 2, but these spectra are acquired in a much shorter measurement time (as mentioned in Table 1).
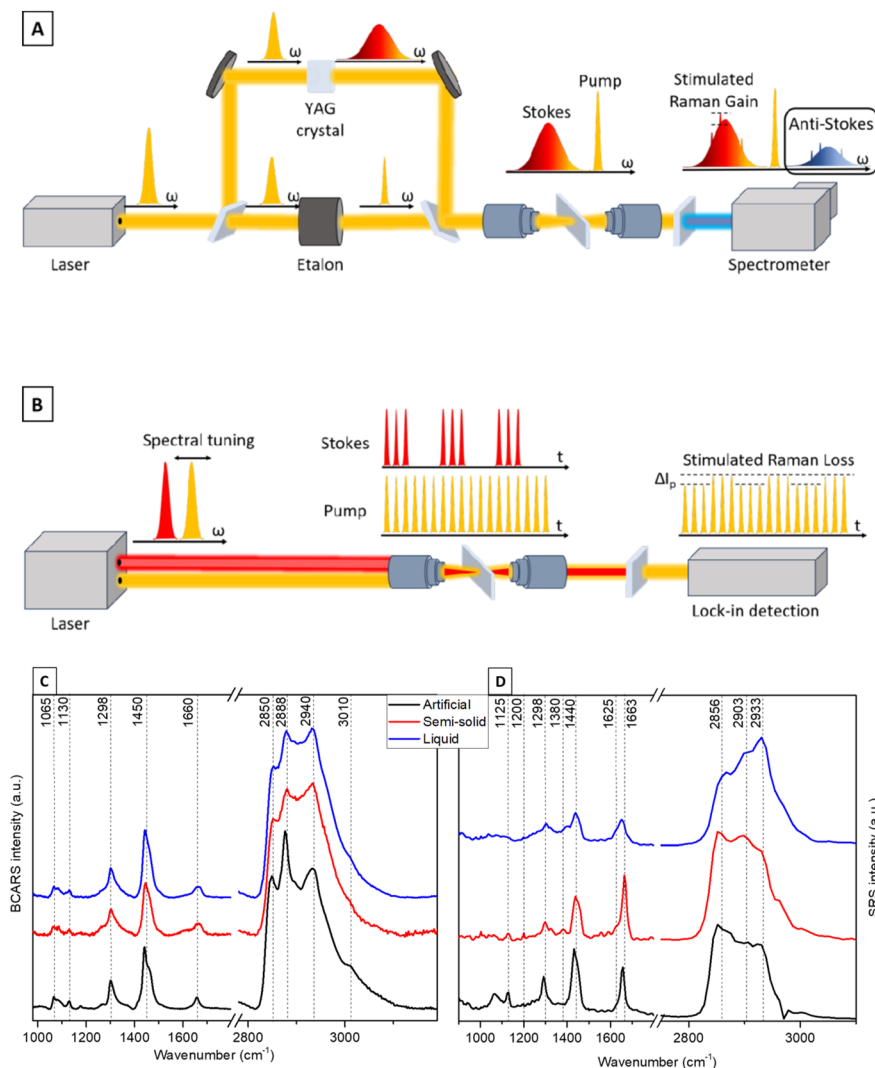
Fig. 4 Schematic illustrations of (A) the home-built BCARS and (B) SRS setups. Averaged (C) BCARS and (D) SRS spectra of artificial (black), semi-solid (red) and liquid (blue) cerumen. Wavenumber range between 900 and 3200 cm^{-1}. The spectra are cut in the silent region between 1800 and 2750 cm^{-1}. Spectra are offset for clarity.

OPTIR analysis as a complementary tool

The Raman analysis presented above shows that Raman spectroscopy mainly displays molecular vibrations of non-polar biomolecules. IR absorption spectroscopy might complement the Raman analysis by also highlighting molecular vibrations exhibiting a large dipole moment, such as those of hydroxyl, carbonyl, and amide bonds present in lipids, proteins, and carbohydrates. Usually, the application of IR spectroscopy to native biomedical specimens is hindered due to the presence of water. In this context, OPTIR spectroscopy in combination with an IR quantum cascade laser offers a solution for also studying aqueous biomedical samples. OPTIR spectroscopy offers high-resolution, non-invasive analysis and enhanced contrast of non-transparent biological samples in reflection on ordinary glass windows as compared to the commonly used FT-IR approach.

Here, we have also applied OPTIR spectroscopy to study human semi-solid, human liquid and artificial cerumen to obtain Raman complementary information about the biomolecular composition of cerumen.

Fig. 5 shows DC and OPTIR hyperspectral images of human semi-solid earwax. The OPTIR imaging mode enables high-resolution exploration of the spatial heterogeneity of the sample by setting the IR laser to two fixed wavenumbers. Here, we have chosen the CH_2 symmetric stretching vibration at 2850 cm^{-1} associated with lipids (Fig. 5B) and the amide I vibration at 1650 cm^{-1} associated with proteins (Fig. 5C). Evidencing the predominant and homogeneous distribution of lipids, OPTIR maps also reveal some protein-rich spots.

A representative OPTIR spectrum of semi-solid cerumen in Fig. 5D (red line) clearly shows the amide II and amide I bands at 1545 and 1650 cm^{-1}, respectively. The band at 1065 cm^{-1} is typical of COH groups,[58] which supports the detection of
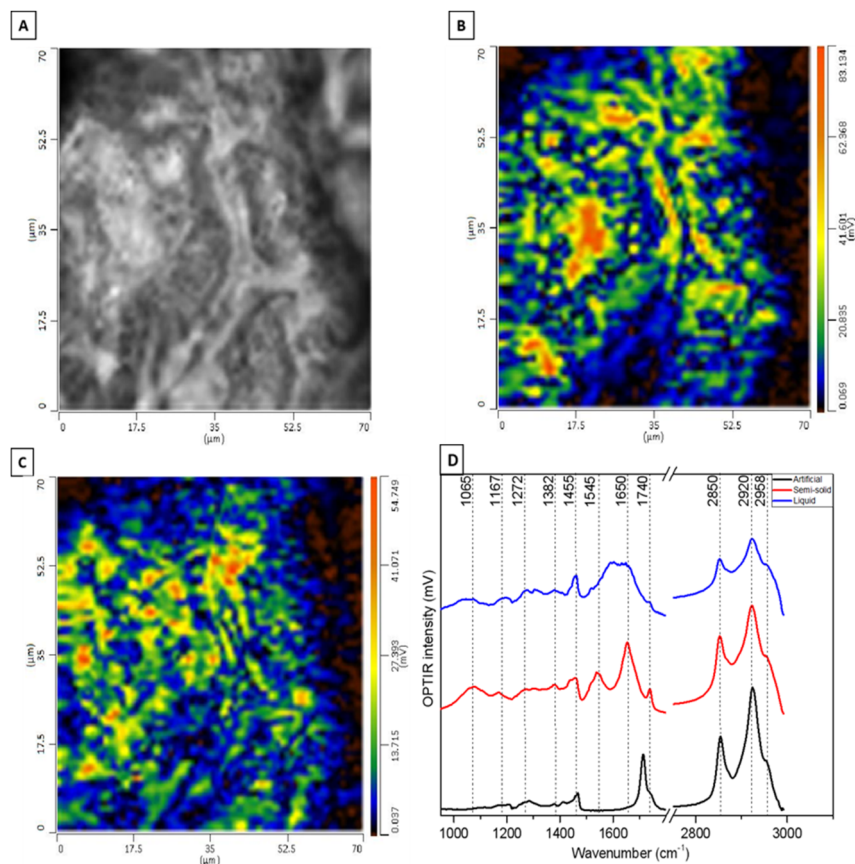
Fig. 5 OPTIR images of semi-solid cerumen. (A) DC image. (B) Lipid distribution: $\nu_{as}(CH_2)$ (2850 cm^{-1}). (C) Protein distribution: amide I (1650 cm^{-1}). (D) OPTIR spectra of artificial (black), semi-solid (red) and liquid (blue) cerumen. Spectral range between 900 and 3000 cm^{-1}. The silent region (1800 and 2700 cm^{-1}) is not covered by the QCL tuning range. Spectra are offset for clarity.

sphingoglycolipids in SRS spectra (Fig. 4D). The lipid C=O stretching band is found at 1740 cm^{-1} in semi-solid cerumen and shifts towards lower wavenumbers for artificial cerumen. The amide bands of proteins are untypically broad, and the C=O band is weak in liquid cerumen. Only typical CH$_2$ bands at 1455 (deformation mode) and 2850/2920 cm^{-1} (stretching modes) are properly resolved and are evident also in the other cerumen OPTIR spectra (Table 2). Some of these vibrational contributions have already been reported by Elkins[59] in a cerumen study through ATR-FTIR spectroscopy. However, OPTIR spectroscopy offers superior identification and lateral resolution capabilities, especially for inhomogeneous specimens.

Discussion

Table 2 summarizes the vibrational spectroscopic cerumen analysis presented above. The main spectral contributions in all samples with all modalities were assigned to lipids, in particular CH$_2$ stretching vibrations in the high wavenumber range. Raman marker bands indicate the degree of unsaturation of fatty acid chains. Raman and IR marker bands of COH groups indicate the presence of sphingoglycolipids that are made up of fatty acid chains and a ceramide backbone linked

to saccharine residues such as galactose. Furthermore, Raman spectra allow detection of typical bands of carotenoids. IR spectra allow detection of the amide bands of proteins that are much weaker in Raman spectra. An indirect detection of lipid-to-protein variations can be achieved by the ratio of CH$_2$ and CH$_3$ stretching vibrations in the high wavenumber range. Protein bands seem to be enhanced in SERS spectra relative to lipid bands. The SERS spectra differ from those obtained using conventional Raman, CARS, SRS, and OPTIR techniques due to the fundamentally distinct principles underlying these methods. Conventional Raman spectroscopy, for example, directly measures vibrational modes based on the inelastic scattering of monochromatic light, without requiring enhancement mechanisms. This results in spectra that reflect the bulk properties of the sample rather than being dominated by surface interactions, as is the case with SERS. In contrast, SERS amplifies the Raman signal of molecules in close proximity to the metal surface, leading to a more surface-specific and often highly sensitive detection of molecular species that might otherwise be undetectable in bulk Raman measurements. This surface selectivity can result in SERS spectra that enhance different vibrational modes or molecular species compared to those observed in conventional Raman spectra.

Additionally, CARS and SRS, which are nonlinear Raman techniques, involve the coherent interaction of multiple laser beams to generate the Raman signal. While these techniques offer high spatial resolution and the ability to selectively probe specific vibrational modes, their operation is based on principles that differ from those of SERS.

The combination of the advanced vibrational spectroscopy techniques may offer a multimodal point-of-care approach, enhancing diagnostic capabilities and enabling comprehensive characterization of body fluids in general. Raman spectroscopy is well established to collect the full molecular fingerprint. Challenges in terms of sensitivity may arise for low-concentration molecules and for those with inherent fluorescent emission that overlap with weaker Raman signals. SERS, in the fingerprint wavenumber region, provides higher detection sensitivity and enables trace-level analysis of specific biomarkers in cerumen media. For the high wavenumber region, SRS and especially BCARS offer unparalleled capabilities for molecular analysis, allowing for the possible detection of variations in lipid and protein content, which is essential information for diagnostic and prognostic tools in cancer liquid biopsies. OPTIR spectroscopy is a variant of IR spectroscopy that gives complementary information to Raman-based methods. Benefits of OPTIR spectroscopy and imaging include data acquisition in reflection mode, sample preparation on inexpensive glass slides, images with submicrometer resolution and spectra with minimal background interference, comparable to established FTIR spectroscopy of thin films or thick samples in attenuated total reflection mode.

Conclusions

Multiple vibrational spectroscopy techniques were applied, offering a powerful approach for the comprehensive analysis of cerumen and shedding light on its complex molecular composition and biological significance. By leveraging the unique strengths of the used vibrational spectroscopic approaches, we uncovered the molecular signatures embedded within cerumen, paving the way for innovative diagnostic methodologies and therapeutic interventions. The insights gained from this interdisciplinary study not only enhance our understanding of cerumen biology but also highlight the potential of vibrational spectroscopy in biomedical research and clinical practice.

The primary goal was to obtain preliminary data that would either support or refute the hypothesis that vibrational spectroscopy could serve as a viable diagnostic approach for cerumen analysis. The successful application of these techniques to the samples from two healthy individuals has provided encouraging results, offering a solid basis for future research that will systematically investigate cerumen samples from a broader population, including those with various health conditions. Ultimately, this study marks the initial step in a promising investigation, setting the stage for more comprehensive research that will assess the clinical utility of vibrational spectroscopy in diagnosing and monitoring health conditions through cerumen analysis. As technology continues to advance, vibrational spectroscopy is poised to revolutionize point-of-care diagnostics, transforming healthcare delivery and improving patient outcomes worldwide.

Author contributions

The manuscript was written through contributions of all authors. Conceptualization: E. F., M. C. and M. S.; sampling and sample preparation: E. F., M. C., J. B. and C. L.; investigation: E. F., M. C., C. M. and M. S. V.; supervision: D. C.-M. and T. M-Z.; writing—original draft preparation: E. F. and M. C.; writing—review and editing: C. K., O. G.-L., M. S., D. C.-M., and J. P.; and funding acquisition: O. G.-L., M. S., and J. P. All authors have given approval to the final version of the manuscript.

Data availability

The data supporting this article have been included as part of the ESI.†

Conflicts of interest

There are no conflicts to declare. The authors declare that they have no known competing financial interests or personal relationships that could have appeared to influence the work reported in this paper.

Acknowledgements

References

1 D. Liu, J. Wang, L. Wu, Y. Huang, Y. Zhang, M. Zhu, Y. Wang, Z. Zhu and C. Yang, Trends in Miniaturized Biosensors for Point-of-Care Testing, *TrAC, Trends Anal. Chem.*, 2020, **122**, 115701, DOI: **10.1016/j.trac.2019.115701**.

2 N. Soda, B. H. A. Rehm, P. Sonar, N.-T. Nguyen and M. J. A. Shiddiky, Advanced Liquid Biopsy Technologies for Circulating Biomarker Detection, *J. Mater. Chem. B*, 2019, **7**(43), 6670–6704, DOI: **10.1039/C9TB01490J.**

3 R. Palmirotta, D. Lovero, P. Cafforio, C. Felici, F. Mannavola, E. Pellè, D. Quaresmini, M. Tucci and F. Silvestris, Liquid Biopsy of Cancer: A Multimodal Diagnostic Tool in Clinical Oncology, *Ther. Adv. Med. Oncol.*, 2018, **10**, DOI: **10.1177/1758835918794630**.

4 X. Zhang and B. Li, Updates of Liquid Biopsy in Oral Cancer and Multiomics Analysis, *Oral Dis.*, 2023, **29**(1), 51–61, DOI: **10.1111/odi.14064**.

5 Z.-H. Qi, H.-X. Xu, S.-R. Zhang, J.-Z. Xu, S. Li, H.-L. Gao, W. Jin, W.-Q. Wang, C.-T. Wu, Q.-X. Ni, X.-J. Yu and L. Liu, The Significance of Liquid Biopsy in Pancreatic Cancer, *J. Cancer*, 2018, **9**(18), 3417–3426, DOI: **10.7150/jca.24591**.

6 D. Di Capua, D. Bracken-Clarke, K. Ronan, A.-M. Baird and S. Finn, The Liquid Biopsy for Lung Cancer: State of the Art, Limitations and Future Developments, *Cancers*, 2021, **13**(16), 3923, DOI: **10.3390/cancers13163923**.

7 B. K. Bhardwaj, S. Thankachan, T. Venkatesh and P. S. Suresh, Liquid Biopsy in Ovarian Cancer, *Clin. Chim. Acta*, 2020, **510**, 28–34, DOI: **10.1016/j.cca.2020.06.047**.

8 A. Alba-Bernal, R. Lavado-Valenzuela, M. E. Domínguez-Recio, B. Jiménez-Rodriguez, M. I. Queipo-Ortuño, E. Alba and I. Comino-Méndez, Challenges and Achievements of Liquid Biopsy Technologies Employed in Early Breast Cancer, *EBioMedicine*, 2020, **62**, 103100, DOI: **10.1016/j.ebiom.2020.103100**.

9 C. Paluszkiewicz, E. Pięta, M. Woźniak, N. Piergies, A. Koniewska, W. Ścierski, M. Misiołek and W. M. Kwiatek, Saliva as a First-Line Diagnostic Tool: A Spectral Challenge for Identification of Cancer Biomarkers, *J. Mol. Liq.*, 2020, **307**, 112961, DOI: **10.1016/j.molliq.2020.112961**.

10 M. A. Feig, E. Hammer, U. Völker and N. Jehmlich, In-Depth Proteomic Analysis of the Human Cerumen—A Potential Novel Diagnostically Relevant Biofluid, *J. Proteomics*, 2013, **83**, 119–129, DOI: **10.1016/j.jprot.2013.03.004**.

11 A. M. Coon, G. Setzen and R. A. Musah, Mass Spectrometric Interrogation of Earwax: Toward the Detection of Ménière's Disease, *ACS Omega*, 2023, **8**(30), 27010–27023, DOI: **10.1021/acsomega.3c01943**.

12 A. M. Coon, A. J. Dane, G. Setzen, R. B. Cody and R. A. Musah, Two-Dimensional Gas Chromatographic and Mass Spectrometric Characterization of Lipid-Rich Biological Matrices—Application to Human Cerumen (Earwax), *ACS Omega*, 2022, **7**(1), 230–239, DOI: **10.1021/acsomega.1c04535**.

13 K. A. Prokop-Prigge, E. Thaler, C. J. Wysocki and G. Preti, Identification of Volatile Organic Compounds in Human Cerumen, *J. Chromatogr. B: Anal. Technol. Biomed. Life Sci.*, 2014, **953–954**, 48–52, DOI: **10.1016/j.jchromb.2014.01.043**.

14 J. F. Guest, M. J. Greener, A. C. Robinson and A. F. Smith, Impacted Cerumen: Composition, Production, Epidemiology and Management, *QJM*, 2004, **97**(8), 477–488, DOI: **10.1093/qjmed/hch082**.

15 M. Schwaab, S. Hansen, A. Gurr, T. Schwaab, A. Minovi, H. Sudhoff and S. Dazert, Protein Isolation from Ear Wax Made Easy, *Eur. Arch. Otorhinolaryngol.*, 2009, **266**(11), 1699–1702, DOI: **10.1007/s00405-009-0960-5**.

16 E. Shokry and N. R. A. Filho, Insights into Cerumen and Application in Diagnostics: Past, Present and Future

Prospective, *Biochem. Med.*, 2017, **27**(3), DOI: **10.11613/BM.2017.030503**.

17 J. M. G. Barbosa, N. Z. Pereira, L. C. David, C. G. de Oliveira, M. F. G. Soares, M. A. G. Avelino, A. E. de Oliveira, E. Shokry and N. R. A. Filho, Cerumenogram: A New Frontier in Cancer Diagnosis in Humans, *Sci. Rep.*, 2019, **9**(1), 11722, DOI: **10.1038/s41598-019-48121-4**.

18 S. P. Chiang, O. H. Lowry and B. H. Senturia, Micro–chemical Studies on Normal Cerumen I. The Lipid and Protein Content of Normal Cerumen as Affected by Age and Sex, *Laryngoscope*, 1955, **65**(10), 927–934, DOI: **10.1288/00005537-195510000-00002**.

19 A. L. Mitchell, K. B. Gajjar, G. Theophilou, F. L. Martin and P. L. Martin–Hirsch, Vibrational Spectroscopy of Biofluids for Disease Screening or Diagnosis: Translation from the Laboratory to a Clinical Setting, *J. Biophotonics*, 2014, **7**(3–4), 153–165, DOI: **10.1002/jbio.201400018**.

20 K. B. Beć, J. Grabska and C. W. Huck, Biomolecular and Bioanalytical Applications of Infrared Spectroscopy – A Review, *Anal. Chim. Acta*, 2020, **1133**, 150–177, DOI: **10.1016/j.aca.2020.04.015**.

21 E. Dumont, C. De Bleye, P.-Y. Sacré, L. Netchacovitch, P. Hubert and E. Ziemons, From Near-Infrared and Raman to Surface-Enhanced Raman Spectroscopy: Progress, Limitations and Perspectives in Bioanalysis, *Bioanalysis*, 2016, **8**(10), 1077–1103, DOI: **10.4155/bio-2015-0030**.

22 D. Pappas, Raman Spectroscopy in Bioanalysis, *Talanta*, 2000, **51**(1), 131–144, DOI: **10.1016/S0039-9140(99)00254-4**.

23 D. Cialla-May, C. Krafft, P. Rösch, T. Deckert-Gaudig, T. Frosch, I. J. Jahn, S. Pahlow, C. Stiebing, T. Meyer-Zedler, T. Bocklitz, I. Schie, V. Deckert and J. Popp, Raman Spectroscopy and Imaging in Bioanalytics, *Anal. Chem.*, 2022, **94**(1), 86–119, DOI: **10.1021/acs.analchem.1c03235**.

24 M. A. Tahir, N. E. Dina, H. Cheng, V. K. Valev and L. Zhang, Surface-Enhanced Raman Spectroscopy for Bioanalysis and Diagnosis, *Nanoscale*, 2021, **13**(27), 11593–11634, DOI: **10.1039/D1NR00708D**.

25 L. Vázquez-Iglesias, G. M. Stanfoca Casagrande, D. García-Lojo, L. Ferro Leal, T. A. Ngo, J. Pérez-Juste, R. M. Reis, K. Kant and I. Pastoriza-Santos, SERS Sensing for Cancer Biomarker: Approaches and Directions, *Bioact. Mater.*, 2024, **34**, 248–268, DOI: **10.1016/j.bioactmat.2023.12.018**.

26 C. Krafft, M. Schmitt, I. W. Schie, D. Cialla-May, C. Matthäus, T. Bocklitz and J. Popp, Label-Free Molecular Imaging of Biological Cells and Tissues by Linear and Nonlinear Raman Spectroscopic Approaches, *Angew. Chem., Int. Ed.*, 2017, **56**(16), 4392–4430, DOI: **10.1002/anie.201607604**.

27 M. Çulha, Raman Spectroscopy for Cancer Diagnosis: How Far Have We Come?, *Bioanalysis*, 2015, **7**(21), 2813–2824, DOI: **10.4155/bio.15.190**.

28 Y. Fan, S. Wang and F. Zhang, Optical Multiplexed Bioassays for Improved Biomedical Diagnostics, *Angew. Chem.*, 2019, **131**(38), 13342–13353, DOI: **10.1002/ange.201901964**.

29 C. W. Freudiger, W. Min, B. G. Saar, S. Lu, G. R. Holtom, C. He, J. C. Tsai, J. X. Kang and X. S. Xie, Label-Free Biomedical Imaging with High Sensitivity by Stimulated Raman Scattering Microscopy, *Science*, 2008, **322**(5909), 1857–1861, DOI: **10.1126/science.1165758**.

30 C. Sandt and F. Borondics, Super-Resolution Infrared Microspectroscopy Reveals Heterogeneous Distribution of Photosensitive Lipids in Human Hair Medulla, *Talanta*, 2023, **254**, 124152, DOI: **10.1016/j.talanta.2022.124152**.

31 T. A. Shaik, A. Ramoji, N. Milis, J. Popp and C. Krafft, Optical Photothermal Infrared Spectroscopy and Discrete Wavenumber Imaging for High Content Screening of Single Cells, *Analyst*, 2023, **148**(22), 5627–5635, DOI: **10.1039/D3AN00902E**.

32 S. I. Meier, S. C. Koelzer, M. Schubert-Zsilavecz and S. W. Toennes, Analysis of Drugs of Abuse in Cerumen – Correlation of Postmortem Analysis Results with Those for Blood, Urine and Hair, *Drug Test. Anal.*, 2017, **9**(10), 1572–1585, DOI: **10.1002/dta.2177**.

33 A. M. Massadeh, N. H. Al-Rawi, M. T. Fayyad, A. M. Shotar, M. I. Al-Farras and S. A. A. Massadeh, Simultaneous Determination of Tramadol in Earwax and Urine Samples: Effects of Age, Duration Time and Sex, *Bioanalysis*, 2024, **16**(6), 363–374, DOI: **10.4155/bio-2023-0217**.

34 C. Krafft, L. Neudert, T. Simat and R. Salzer, Near Infrared Raman Spectra of Human Brain Lipids, *Spectrochim. Acta, Part A*, 2005, **61**(7), 1529–1535, DOI: **10.1016/j.saa.2004.11.017**.

35 A. Rygula, K. Majzner, K. M. Marzec, A. Kaczor, M. Pilarczyk and M. Baranska, Raman Spectroscopy of Proteins: A Review, *J. Raman Spectrosc.*, 2013, **44**(8), 1061–1076, DOI: **10.1002/jrs.4335**.

36 E. Farnesi, S. Rinaldi, C. Liu, J. Ballmaier, O. Guntinas-Lichius, M. Schmitt, D. Cialla-May and J. Popp, Label-Free SERS and MD Analysis of Biomarkers for Rapid Point-of-Care Sensors Detecting Head and Neck Cancer and Infections, *Sensors*, 2023, **23**(21), 8915, DOI: **10.3390/s23218915**.

37 I. Bruzas, W. Lum, Z. Gorunmez and L. Sagle, Advances in Surface-Enhanced Raman Spectroscopy (SERS) Substrates for Lipid and Protein Characterization: Sensing and Beyond, *Analyst*, 2018, **143**(17), 3990–4008, DOI: **10.1039/C8AN00606G**.

38 D. Polli, V. Kumar, C. M. Valensise, M. Marangoni and G. Cerullo, Broadband Coherent Raman Scattering Microscopy, *Laser Photonics Rev.*, 2018, **12**(9), DOI: **10.1002/lpor.201800020**.

39 Y. Liu, Y. J. Lee and M. T. Cicerone, Broadband CARS Spectral Phase Retrieval Using a Time-Domain Kramers–Kronig Transform, *Opt. Lett.*, 2009, **34**(9), 1363, DOI: **10.1364/OL.34.001363**.

40 C. H. Camp, Y. J. Lee and M. T. Cicerone, Quantitative, Comparable Coherent Anti–Stokes Raman Scattering (CARS) Spectroscopy: Correcting Errors in Phase Retrieval, *J. Raman Spectrosc.*, 2016, **47**(4), 408–415, DOI: **10.1002/jrs.4824**.

41 M. Brinkmann, A. Fast, T. Hellwig, I. Pence, C. L. Evans and C. Fallnich, Portable All-Fiber Dual-Output Widely Tunable Light Source for Coherent Raman Imaging, *Biomed. Opt. Express*, 2019, **10**(9), 4437, DOI: **10.1364/BOE.10.004437**.

42 B. Manifold and D. Fu, Quantitative Stimulated Raman Scattering Microscopy: Promises and Pitfalls, *Annu. Rev. Anal. Chem.*, 2022, **15**(1), 269–289, DOI: **10.1146/annurev-anchem-061020-015110**.

43 H. Rosales-Solano, V. Galievsky, K. Murtada, P. V. Radovanovic and J. Pawliszyn, Profiling of Unsaturated Lipids by Raman Spectroscopy Directly on Solid-Phase Microextraction Probes, *Anal. Chem.*, 2022, **94**(2), 606–611, DOI: **10.1021/acs.analchem.1c04054**.

44 Y. Xiong, Y. Si, Y. Feng, S. Zhuo, B. Cui and Z. Zhang, Prognostic Value of Lipid Metabolism–related Genes in Head and Neck Squamous Cell Carcinoma, *Immun., Inflammation Dis.*, 2021, **9**(1), 196–209, DOI: **10.1002/iid3.379**.

45 J. Schmidt, B. Kajtár, K. Juhász, M. Péter, T. Járai, A. Burián, L. Kereskai, I. Gerlinger, T. Tornóczki, G. Balogh, L. Vígh, L. Márk and Z. Balogi, Lipid and Protein Tumor Markers for Head and Neck Squamous Cell Carcinoma Identified by Imaging Mass Spectrometry, *Oncotarget*, 2020, **11**(28), 2702–2717, DOI: **10.18632/oncotarget.27649**.

46 M. Köhler, S. Machill, R. Salzer and C. Krafft, Characterization of Lipid Extracts from Brain Tissue and Tumors Using Raman Spectroscopy and Mass Spectrometry, *Anal. Bioanal. Chem.*, 2009, **393**(5), 1513–1520, DOI: **10.1007/s00216-008-2592-9**.

47 K. Hanna, E. Krzoska, A. M. Shaaban, D. Muirhead, R. Abu-Eid and V. Speirs, Raman Spectroscopy: Current Applications in Breast Cancer Diagnosis, Challenges and Future Prospects, *Br. J. Cancer*, 2022, **126**(8), 1125–1139, DOI: **10.1038/s41416-021-01659-5**.

48 A. Y. F. You, M. S. Bergholt, J.-P. St-Pierre, W. Kit-Anan, I. J. Pence, A. H. Chester, M. H. Yacoub, S. Bertazzo and M. M. Stevens, Raman Spectroscopy Imaging Reveals Interplay between Atherosclerosis and Medial Calcification in the Human Aorta, *Sci. Adv.*, 2017, **3**(12), DOI: **10.1126/sciadv.1701156**.

49 M. S. Schmidt, J. Hübner and A. Boisen, Large Area Fabrication of Leaning Silicon Nanopillars for Surface Enhanced Raman Spectroscopy, *Adv. Mater.*, 2012, **24**(10), DOI: **10.1002/adma.201103496**.

50 L. Morelli, K. Zór, C. B. Jendresen, T. Rindzevicius, M. S. Schmidt, A. T. Nielsen and A. Boisen, Surface Enhanced Raman Scattering for Quantification of *p*-Coumaric Acid Produced by *Escherichia Coli*, *Anal. Chem.*, 2017, **89**(7), 3981–3987, DOI: **10.1021/acs.analchem.6b04428**.

51 L. Shen, Y. Du, N. Wei, Q. Li, S. Li, T. Sun, S. Xu, H. Wang, X. Man and B. Han, SERS Studies on Normal Epithelial and Cancer Cells Derived from Clinical Breast Cancer

Specimens, *Spectrochim. Acta, Part A*, 2020, **237**, 118364, DOI: **10.1016/j.saa.2020.118364**.

52 H. Abramczyk and B. Brozek-Pluska, New Look inside Human Breast Ducts with Raman Imaging. Raman Candidates as Diagnostic Markers for Breast Cancer Prognosis: Mammaglobin, Palmitic Acid and Sphingomyelin, *Anal. Chim. Acta*, 2016, **909**, 91–100, DOI: **10.1016/j.aca.2015.12.038**.

53 H. Hajab, A. Anwar, H. Nawaz, M. I. Majeed, N. Alwadie, S. Shabbir, A. Amber, M. I. Jilani, H. F. Nargis, M. Zohaib, S. Ismail, A. Kamal and M. Imran, Surface-Enhanced Raman Spectroscopy of the Filtrate Portions of the Blood Serum Samples of Breast Cancer Patients Obtained by Using 30 kDa Filtration Device, *Spectrochim. Acta, Part A*, 2024, **311**, 124046, DOI: **10.1016/j.saa.2024.124046.**

54 S. Werner, L. Keller and K. Pantel, Epithelial Keratins: Biology and Implications as Diagnostic Markers for Liquid Biopsies, *Mol. Aspects Med.*, 2020, **72**, 100817, DOI: **10.1016/j.mam.2019.09.001**.

55 F. Vernuccio, R. Vanna, C. Ceconello, A. Bresci, F. Manetti, S. Sorrentino, S. Ghislanzoni, F. Lambertucci, O. Motiño, I. Martins, G. Kroemer, I. Bongarzone, G. Cerullo and D. Polli, Full-Spectrum CARS Microscopy of Cells and Tissues with Ultrashort White-Light Continuum Pulses,

J. Phys. Chem. B, 2023, **127**(21), 4733–4745, DOI: **10.1021/acs.jpcb.3c01443**.

56 A. De la Cadena, F. Vernuccio, A. Ragni, G. Sciortino, R. Vanna, C. Ferrante, N. Pediconi, C. Valensise, L. Genchi, S. P. Laptenok, A. Doni, M. Erreni, T. Scopigno, C. Liberale, G. Ferrari, M. Sampietro, G. Cerullo and D. Polli, Broadband Stimulated Raman Imaging Based on Multi-Channel Lock-in Detection for Spectral Histopathology, *APL Photonics*, 2022, 7(7), DOI: **10.1063/5.0093946.**

57 T. Meyer, M. Chemnitz, M. Baumgartl, T. Gottschall, T. Pascher, C. Matthäus, B. F. M. Romeike, B. R. Brehm, J. Limpert, A. Tünnermann, M. Schmitt, B. Dietzek and J. Popp, Expanding Multimodal Microscopy by High Spectral Resolution Coherent Anti-Stokes Raman Scattering Imaging for Clinical Disease Diagnostics, *Anal. Chem.*, 2013, **85**(14), 6703–6715, DOI: **10.1021/ac400570w.**

58 I. Dreissig, S. Machill, R. Salzer and C. Krafft, Quantification of Brain Lipids by FTIR Spectroscopy and Partial Least Squares Regression, *Spectrochim. Acta, Part A*, 2009, **71**(5), 2069–2075, DOI: **10.1016/j.saa.2008.08.008.**

59 K. M. Elkins, Rapid Presumptive "Fingerprinting" of Body Fluids and Materials by ATR FT–IR Spectroscopy, *J. Forensic Sci.*, 2011, **56**(6), 1580–1587, DOI: **10.1111/j.1556-4029.2011.01870.x.**